Ocean Engineering 60 (2013) 208–218

Contents lists available at SciVerse ScienceDirect

Ocean Engineering

journal homepage: www.elsevier.com/locate/oceaneng

Centrifuge modeling of steel catenary risers at touchdown zone part II: Assessment of centrifuge test results using kaolin clay

Bradley J. Elliott [a,b], Arash Zakeri [c,*], John Barrett [a], Bipul Hawlader [b], George Li [d], Edward C. Clukey [c]

[a] C-CORE, Captain Robert A. Bartlett Building, Morrissey Rd, St. John's, NL, Canada
[b] Faculty of Engineering and Applied Science, Memorial University of Newfoundland, St. John's, NL, Canada
[c] BP America, 501 Westlake Park Boulevard, Houston, TX, USA
[d] Shell International Exploration and Production Inc., 200N. Diary Ashford, Houston, TX, USA

ARTICLE INFO

Available online 29 December 2012

Keywords:
Steel catenary riser (SCR)
Touchdown zone
Fatigue
Riser–soil interaction
Centrifuge modeling

ABSTRACT

This paper presents the results of an experimental investigation into the fatigue issues related to steel catenary risers (SCRs) within the Touchdown Zone (TDZ). The experiment was conducted in the C-CORE geotechnical centrifuge using the apparatus described in Part I (the companion paper). Kaolin clay with an undrained shear strength profile typical of deepwater Gulf of Mexico was used for the model seabed. The model riser simulated an approximately 108 m long, 0.5 m diameter SCR subjected to four sets of synthetic heave and surge motions ranging in complexity from a simple sinusoidal wave to those having characteristics of dual frequency Response-Amplitude-Operator (RAO) motions. The results provided valuable insights into the fluid–riser–soil interaction mechanism, trench formation and its influence on the fatigue stresses of an SCR. The results indicated that the trench geometry had a significant influence on the fatigue stresses. The formation of the trench in this experimental program resulted in considerable reduction (as high as about 20%) in bending and tensile fatigue stresses. The experimental program demonstrated that the fatigue life of an SCR could potentially increase as the trench developed from its original mudline state.

1. Introduction

This paper presents the results of a series of experiments conducted in a geotechnical centrifuge as part of a large research program aiming to investigate fatigue damage on a Steel Catenary Riser (SCR) within the Touchdown Zone (TDZ). The overall objective of the program was to develop a testing apparatus to simulate an SCR within the TDZ subjected to various motions representative to those induced by a floating platform in storm conditions, to understand the riser–fluid–soil interaction mechanism, and to investigate the influence of the resulting trench on the fatigue life of the riser. The results of this research program are summarized in two papers. Part I (Elliott et al., this issue) describes the development of the testing apparatus, scaling of the experiments, and the procedures for the validation of the model riser on an elastic seabed and the associated Finite Element Analysis (FEA). This paper, Part II, describes preparation of the model seabed, the riser motions and testing procedures, and test results. All results herein are presented in model terms unless otherwise noted. Most figures present the results in both model and prototype terms. The scaling laws and conversions are provided in Part I.

2. Physical setup and design parameters

2.1. Model riser properties and boundary conditions

The riser geometry and material properties remained unchanged from the elastic seabed test described in Elliott et al. this issue. The model riser was made of commercially available stainless steel tubing, with an outside diameter of 12.7 mm and a wall thickness of 0.711 mm (508 mm and 28.4 mm, respectively, in prototype terms). It was instrumented with strain gauges, filled with canola oil (to achieve the targeted submerged unit weight), and encased with a heat shrink to protect the underlying strain gauges. The instrumented model riser with the heat shrink had an outside diameter of 14.1 mm and a submerged unit weight of 67.3 N/m (2.69 kN/m in prototype terms). The modulus of elasticity of the riser was determined to be 210 GPa through the use of ASTM standard tensile tests.

2.2. Riser boundary conditions

A pin and roller bearing connected the motion-end of the riser to the X–Z stage to allow it to freely rotate in pitch, the axis

* Corresponding author. Formerly at C-CORE. Tel.: +1 713 323 2420; fax: +281 366 7969
E-mail addresses: arash.zakeri@bp.com, azakeri@mun.ca (A. Zakeri).

0029-8018/$ - see front matter © 2012 Elsevier Ltd. All rights reserved.
http://dx.doi.org/10.1016/j.oceaneng.2012.11.013

normal to the plane of the applied heave and surge motions. At the fixed-end, the riser was connected to an upstand attached to the test box with a clamp and counterweighted linear guide block system. The fixed-end was free to translate vertically, following consolidation and self-trenching deformations, and to rotate in pitch about the axis normal to the plane of the heave and surge motions. The height of the upstand was adjusted to achieve an axial stiffness of 881 N/mm (35.24 MN/m in prototype terms) in the riser.

2.3. Model seabed preparation and properties

Kaolin clay was used to make the model seabed. The clay was reconstituted from a slurry having a moisture content of 120% (twice the Liquid Limit), and consolidated to a final depth of 77 mm under a vertical effective stress of 55 kPa to achieve the target undrained shear strength. The target strength profile consisted of 4 kPa crust to about 600–800 mm depth (15–20 mm in model scale) increasing at a rate of 1.6 kPa/m below the crust. This profile was thought to be representative of deepwater conditions in the Gulf of Mexico and was similar to conditions used by others in SCR studies (Aubeny and Biscontin, 2009).

2.4. Applied motions

Four sets of artificial motions were applied to the model riser to investigate the trench formation mechanisms (such as erosion and rate effects) and the influence of trench depths on fatigue stresses. Each motion had a different amplitude and frequency and was applied in the heave and surge directions, illustrated in Fig. 1 in model terms. For all motions, the heave to surge ratio was fixed at 14 and positive surge induced tension in riser (i.e., away from the fixed-end) and positive heave resulted in displacement up and away from seabed. The first motion (M1) consisted of a simple sinusoidal function with heave and surge amplitudes of 30.0 mm and 2.11 mm, respectively, both having a frequency of 0.05 Hz. The second motion (M2) was developed to include a higher superimposed secondary frequency in the applied motion without increasing the overall amplitude.

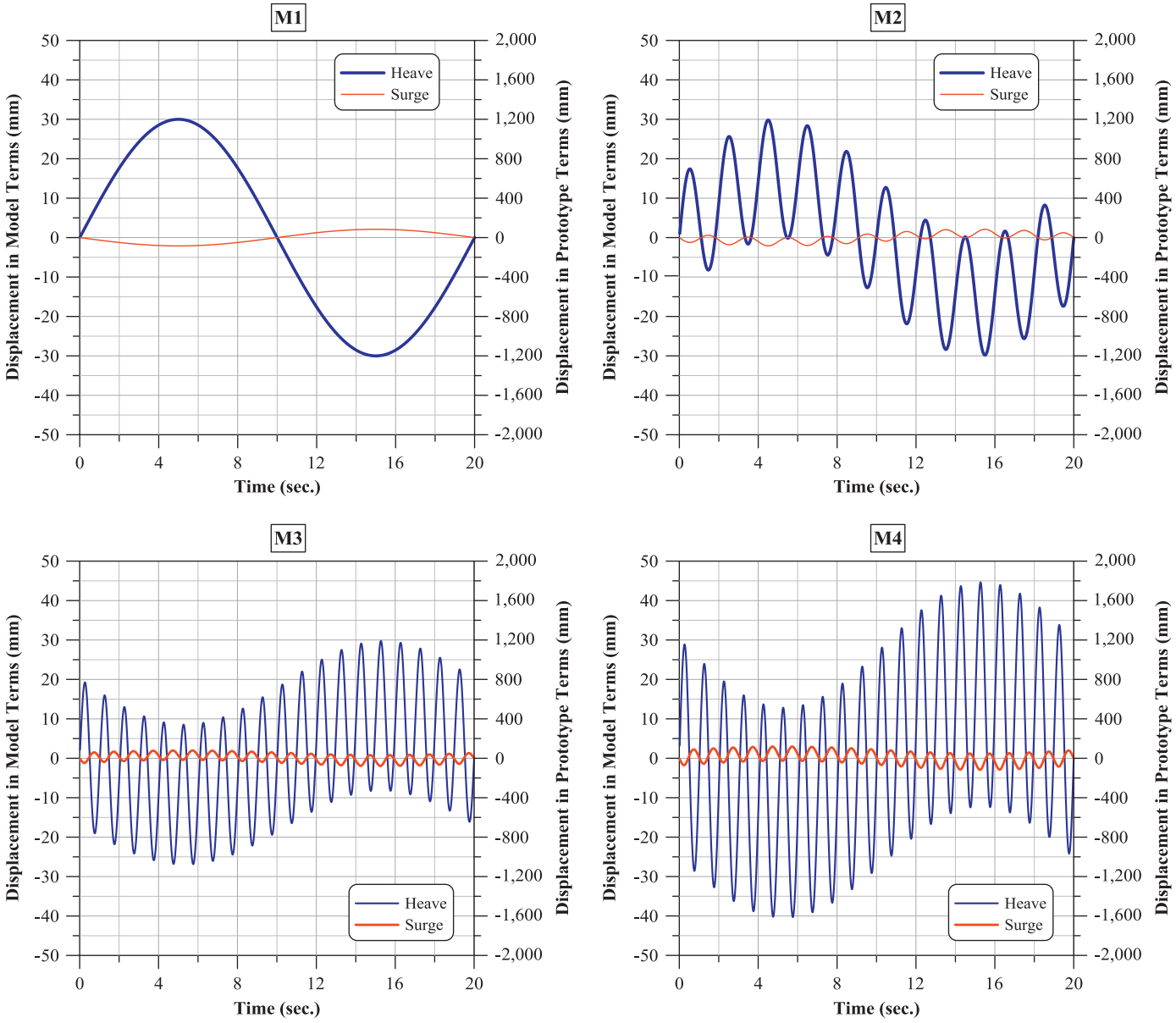

Fig. 1. Motions used in centrifuge test: M1 (top, left), M2 (top, right), M3 (bottom, left), and M4 (bottom, right).

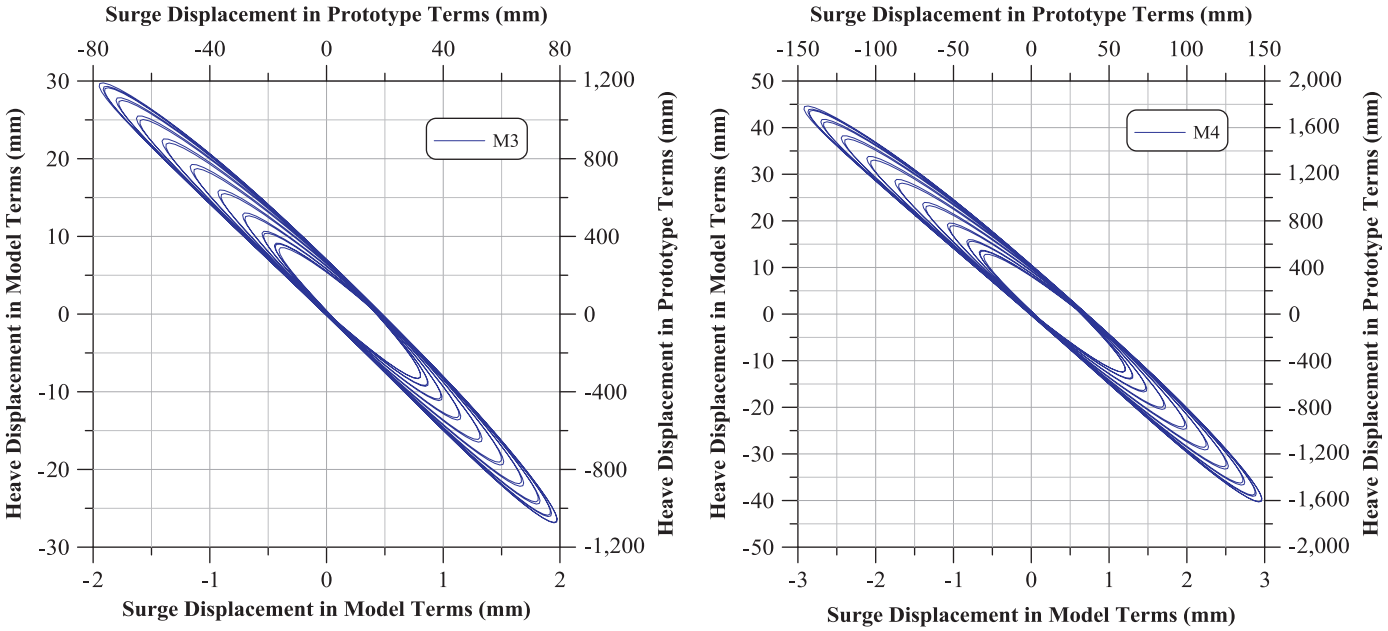

Fig. 2. Heave versus surge displacements: M3 motion (left) and M4 motion (right). Note the difference in scales.

To obtain a more representative riser motion in the TDZ of the model, a simple oscillating wave motion was translated along the length of the riser from the water surface to 4.9 m above the seabed, in prototype scale. This created a complex dual frequency waveform, shown in Fig. 1(c) and (d) in model scale, with frequencies of 0.05 Hz and 1 Hz. The heave and surge neutral axes were shifted upwards by 2.89 mm and the surge was phased shifted by 0.26 s from the heave motion, shown by the separation from the linear line in Fig. 2. The fourth motion (M4) increased the magnitudes of the surge and heave displacements of M3 by 50% without changing the frequencies or phase shifts. M3 and M4 are motions characteristic of a riser induced by a floating platform in storm conditions, however, are purely artificial and do not represent any specific geographic location.

3. Instrumentation

Fig. 3 presents the instrumentation layout of the model riser and the clay seabed. A complete description of all instruments used during the test series is provided in Sections 3.1–3.4.

3.1. Pore pressure transducer

Seven miniature Pore Pressure Transducers (PPTs) were used. Two PPTs were installed on the surface of the clay to measure the height of the free surface water, two PPTs were installed at approximately half the clay depth to measure the dissipation of excess pore pressures during consolidation, and four PPTs were installed in close proximity to the riser at depths of two, three, and four times the riser diameter.

3.2. Displacement measurements

In addition to the PPTs installed in the clay, consolidation was also monitored using two Linear Variable Differential Transformers (LVDTs) on the clay surface at opposite ends of the test box. Two additional LVDTs were mounted on the riser at the fixed-end using extension rods with semi-circular cradles, separated by a distance of 24 mm. This allowed for both the settlement and the inclination of the riser at the fixed-end to be measured. Lasers were also used to measure the settlement and displacement of the riser at 0.8 m (Laser 1) and 1.6 m (Laser 2) from the fixed-end. Each laser system consisted of a small freely sliding plate that was connected to the riser with a string and pulley. The laser beam reflected from the plate and allowed measurement of the riser and trench deformations during the tests.

3.3. Inclinometers

Two inclinometers were used during these tests, one attached to the test box to measure the rotation of the centrifuge swing and a second attached to the motion-end clamp to measure the inclination of the riser at the pickup point.

3.4. Riser

The riser was instrumented with 22 full bridge strain gauge pairs; 18 oriented to measure the bending response of the riser, and three to measure the riser tension (strain gauge 21 (SG21) at the fixed-end and SG1 and SG1b at the motion-end). Two additional full bridge pairs were installed on the truss members, connecting the riser to the X–Z stage. These gauges measured the horizontal component of the riser tension and the resultant tension was calculated by the truss response corrected by using the inclination measured by the inclinometer attached to the motion-end clamp. The locations of the strain gauges along the length of the riser are given in Table 1.

4. Procedures for centrifuge tests

The following is a summary of all the test procedures developed by C-CORE for this centrifuge testing program, including setup, consolidation, lifting and lowering of the riser, application of motions, and soil characterization tests.

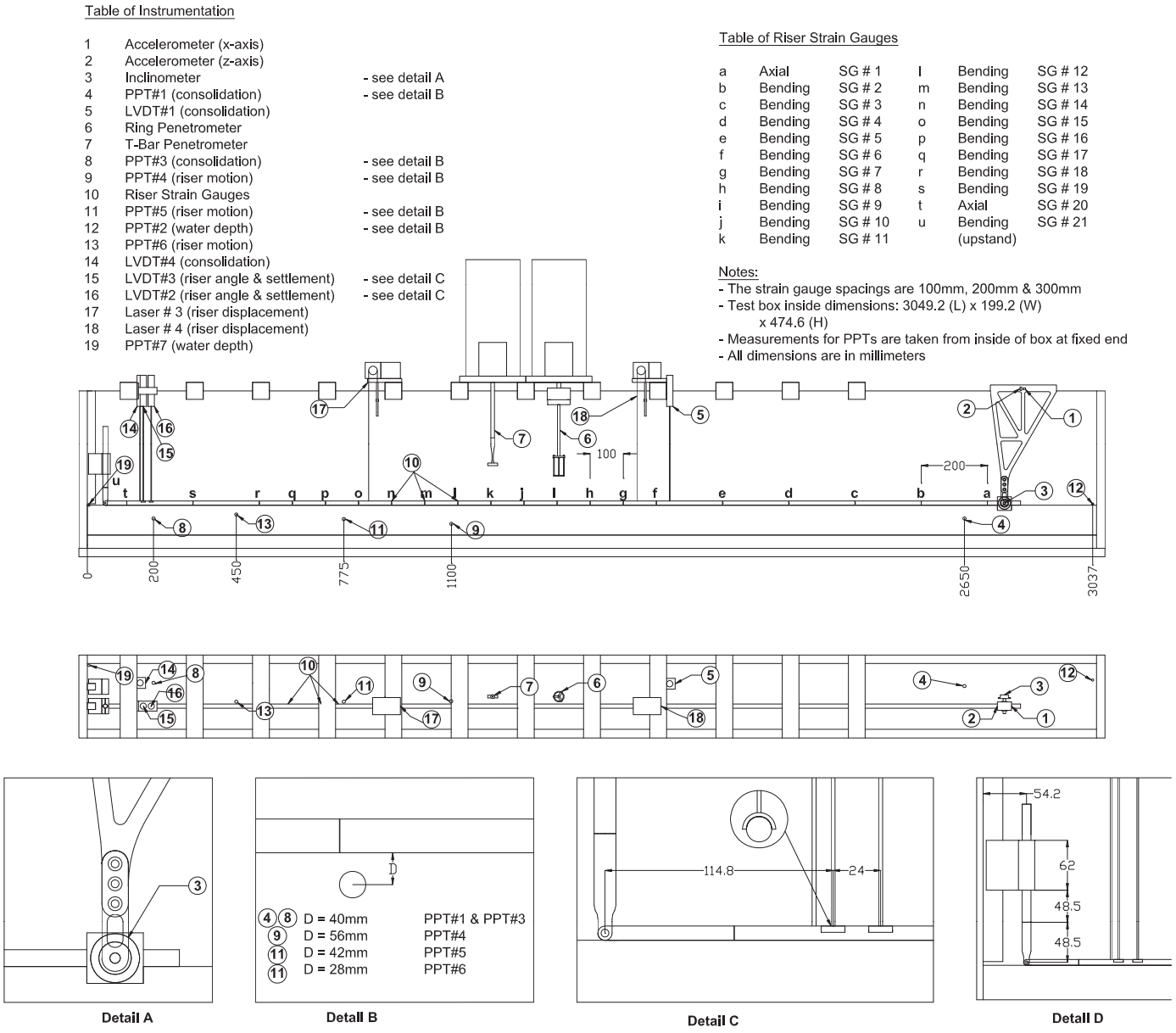

Fig. 3. Instrumentation layout with clay bed.

4.1. Consolidation phase

Spin centrifuge up to test speed (40 g). Monitor riser tension and adjust accordingly to maintain a tension of approximately 100 N.

Monitor PPTs installed in the clay for dissipation of excess pore pressure, and LVDTs for surface settlement until 95% consolidation is achieved; verified by using the root time method.

4.2. Applied motions

- Lift the riser until the centerline is 120 mm above the clay surface at the motion-end while maintaining a tension of approximately 100 N.
- Tension riser to the target tension (350 N) at the motion-end by adjusting the surge axis of the X–Z stage.
- Increase the data acquisition sampling rate to 40 Hz.
- Apply the motions in packets, each packet having 20 cycles, separated by period of 30 s. The sequence of motions is summarized in Table 2. Also, see Figs. 1, 2, and 4 for further details of the applied motions.
- Lower riser until the centerline of the riser is 13 mm above the clay surface at the motion-end while maintaining a tension of approximately 100 N.

4.3. Soil characterization tests

- Activate the T-bar vertical drive at 3 mm/s to obtain the clay strength profile.
- Cycle the T-bar cycled up/down (10 cycles) to measure the remolded strength profile of the clay.
- Activate the ring penetrometer vertical drive at 10 mm/s to obtain the clay strength profile.
- Cycle the ring penetrometer up/down (10 cycles) to measure the remolded strength of the clay.

4.4. End of test/post test measurements

- Centrifuge stop – spin down to 1 g.

- Core samples of the clay were taken at opposite ends of the test box and measured for moisture content per 10 mm depth increments.
- The clay was digitized using a coordinate measuring machine (CMM).

Table 1
Riser strain gauge locations.

Strain Gauge	Measurement	Distance from motion pin (mm)	Strain Gauge	Measurement	Distance from motion pin (mm)
Truss	Tension	0	SG # 11	Bending	1651.5
SG # 1	Tension	51.5	SG # 12	Bending	1751.5
SG # 1b	Tension	201.5	SG # 13	Bending	1851.5
SG # 2	Bending	351.5	SG # 14	Bending	1951.5
SG # 3	Bending	551.5	SG # 15	Bending	2051.5
SG # 4	Bending	751.5	SG # 16	Bending	2151.5
SG # 5	Bending	951.5	SG # 17	Bending	2251.5
SG # 6	Bending	1151.5	SG # 18	Bending	2351.5
SG # 7	Bending	1251.5	SG # 19	Bending	2451.5
SG # 8	Bending	1351.5	SG # 20	Tension	2651.5
SG # 9	Bending	1451.5	SG # 21	Tension	2716.6
SG # 10	Bending	1551.5			

Table 2
Testing sequence.

Motion	Packets	Cycles	Duration (min)
M1	3	60	20
M2	3	60	20
M3	3	60	20
M4	3	60	20
M2	3	60	20

5. Test results and discussion

5.1. Heave and surge motions

Following completion of the in-flight consolidation, the riser was lifted to 120 mm above the seabed, equivalent to 4.9 m in prototype terms, and tensioned to approximately 350 N. After tensioning riser, the surge and heave motions were applied. Fig. 4 illustrates the motions applied and their sequences. Each packet of motion contained 20 cycles of and was separated by a 30 s interval to allow for excess pore pressures to dissipate.

5.2. Shear strength of model seabed

The clay consolidated under 40 g for a period of 2.7 h reaching 95% consolidation at 1.83 h with an overall settlement of 1.2 mm. Ninty-five percent consolidation was chosen to ensure almost no excess pore pressure exist prior to applying the motions. The water level above the clay and the excess pore pressures were also monitored. The undrained shear strengths (s_u) were measured in-flight at two locations using a miniature T-bar and a ring penetrometer. The T-bar was 8 mm in diameter and 30 mm in length. The ring penetrometer, developed at C-CORE, was essentially a 2.4 mm diameter stainless steel wire formed into a 35 mm diameter ring. It had the same operational principles as the T-bar, with the advantage of being able to measure s_u at shallower depths. The T-bar and ring penetrometer were inserted into the clay at rates equal to 3 mm/s and 10 mm/s, respectively, calculated based on the recommendations made by Finnie and Randolph (1994). It should be noted that rate effects are important and needed to be considered. For example, an increase by a factor of just over 10 would be expected to give strengths some 20% higher (e.g. Lehane et al., 2009).

The measured and targeted s_u and moisture content profiles are shown in Fig. 5(a) and (b), respectively. The clay had an average residual shear strength of 2.9 kPa and an average moisture content of 69%. The ring penetrometer measured slightly higher shear strengths below 10 mm depth, caused by the resistances in the three upstands due to the design and location of the load cell. The T-bar load cell was located immediately above the cross bar and measured only the resistance created by the flow of clay around the bar, whereas the ring penetrometer load cell was located on a cruciform connected to the ring by three 2.4 mm diameter rods and was affected by the resistance of the rods as they passed through the clay. It should be noted that the ring penetrometer was designed to measure s_u within the upper 10 mm only.

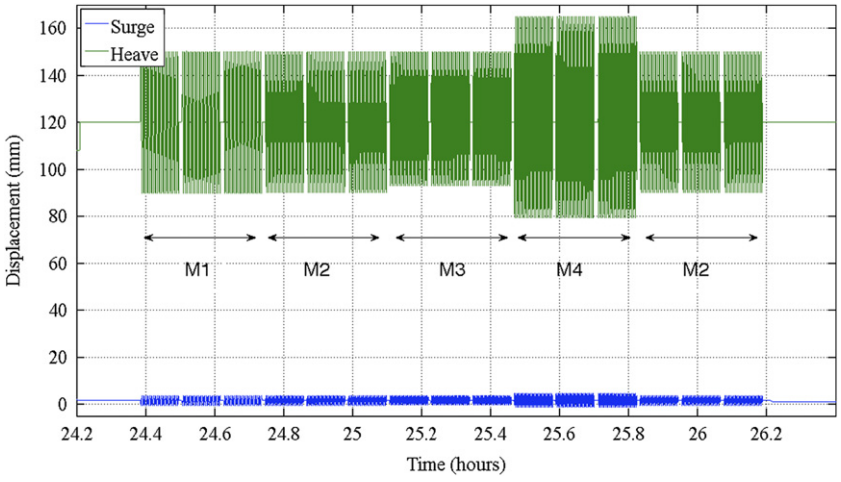

Fig. 4. Applied motions.

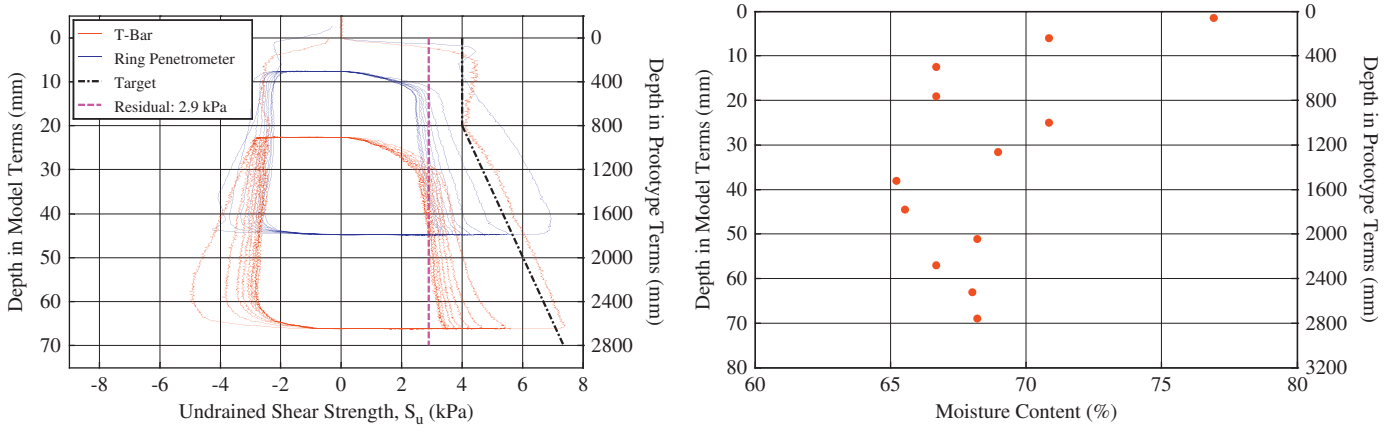

Fig. 5. Undrained shear strength (a) and water content (b) profiles in model terms (*note*: zero on the *y*-axis corresponds to mudline).

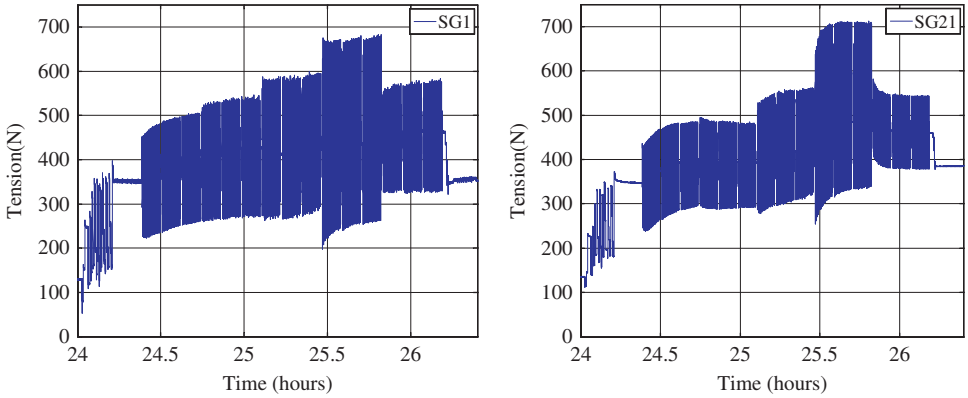

Fig. 6. Tension of SG1 (left) and SG21 (right) during applied motions. From the left, each three sets represent M1, M2, M3, M4 and M2 motions, respectively.

5.3. Tension forces

Fig. 6 presents the tensions measured by SG1 and SG21 (see Fig. 3 for location) at the motion-end and fixed-end, respectively. The tension forces at the fixed-end were lower than those measured at the motion-end because of the catenary action and partly due to the axial friction in the trench and surface zone. During the M1 and M2 motions, there was an increase in the tensions as the trench was formed and as its depth increased with time. The overall amplitude of the M3 motion was slightly smaller than those of the M1 and M2 in the downward direction, however, the out-of-phased surge created higher tensions in the riser. Further, the increase in tension measured by SG21 suggested that the trench geometry changed and the deepest point shifted towards the fixed-end during the M3 motion. The M4 motion had the largest overall amplitude, which were reflected in the tension measured as the trench increased in depth. The tension magnitudes dropped and remain constant during the last M2 motion, which indicated that the trench had reached a steady-state condition and its geometry did not changing significantly.

5.4. Bending moments

Fig. 7 shows the bending moments measured by the strain gauges in model terms. SG14 and SG19 were unresponsive during the centrifuge test and thus are not shown. Fig. 8 presents the bending moment profiles taken before and after implementation of each series of motions. The influence of trench formation and increase in trench depth as the motions were applied were clearly evident from this figure. The magnitude of the bending moments in the fatigue critical zone near touchdown point decreased as the trench depth increased (see Section 5.5 for trench data) and with this, the point of maximum moment shifted towards the fixed-end. The zone where is critical with regards to fatigue stresses occurs between SG 3 and SG9. The two kinks in the bending moment profiles near SG8 and SG12 were caused by the strings attached to the riser as part of the laser measuring system (Fig. 8), which applied a nominal point load of 2.1 N.

Strain gauges SG9, SG10, and SG11 measured the largest peak-to-trough magnitudes of bending moments, which correspond to a zone where fatigue damage would be most significant (discussed in Section 5.8). Fig. 9(a) presents the bending moments measured in SG10 during the M1 motion. Fig. 9(b) shows the difference between the consecutive maximum and minimum values (peaks and troughs) measured during all the motions for SG10.

5.5. Trench data

Fig. 10 shows the measurements made by Lasers 1 and 2. The laser applied a nominal load of 2.1 N at the point of connection to the riser. The sinusoidal M1 motion formed the initial trench. The M2 motion was a combination of two sine functions with in-phased heave and surge; however, it did not represent realistic storm characteristics and was only applied to investigate erosion caused by agitating the water in vicinity of the riser. The amplitude of the M2 motion was the same as M1 but contained a higher frequency component. This secondary frequency did not have a significant influence on the trench formation. The M3 motion increased the depth of the trench despite having slightly smaller overall amplitude in the downward

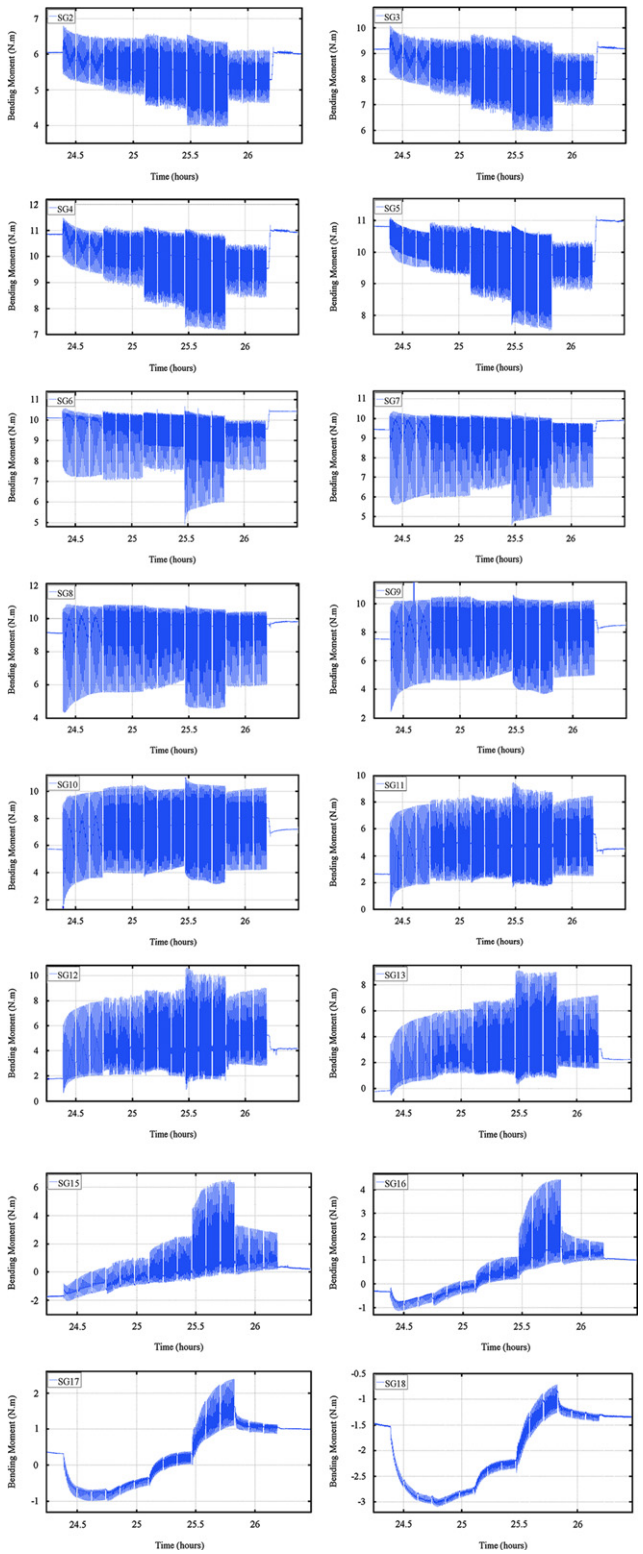

Fig. 7. Response of bending strain gauges. (Note: scale of the vertical axis is different.) From the left, each three sets represent M1, M2, M3, M4 and M2 motions, respectively.

direction than the M1 and M2 motions. The M4 motion, the largest motion, increased the depth of the trench and reached steady-state condition towards the end.

Upon completion of the test, excess water was removed from the clay surface and the final trench and berm geometries were digitally scanned using a coordinate measuring machine (CMM).

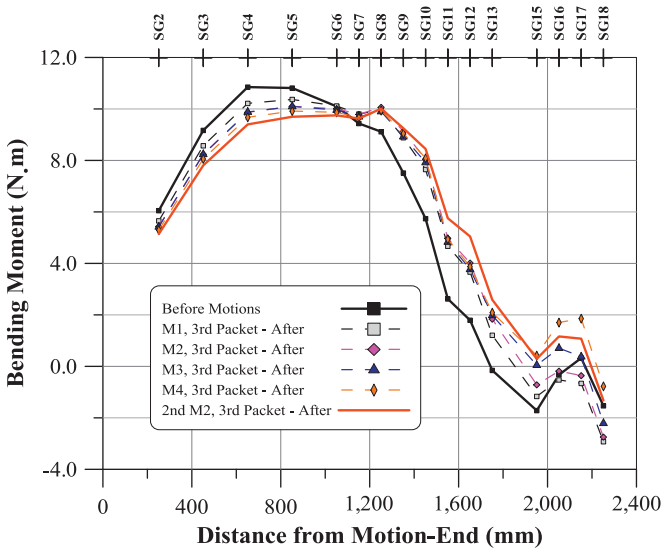

Fig. 8. Bending moment profiles before and after motions.

Figs. 11 and 12 show the three-dimensional and plan views of the final trench and berm geometries as measured by the CMM. The color bars shown in the figures indicate depth in mm.

Fig. 13 presents the mudline, trench, and berm geometries. At its greatest depth, the trench was approximately equal to the diameter of the riser. ROV field observations show that the trench could be as deep as three to four times the riser diameter. It is likely that the erosion caused by the water velocity field around the riser plays a significant role in the trench formation mechanism. It appears this erosion aspect was not fully captured in this test, and therefore, it is postulated that this aspect of the fluid–riser–soil interaction was not properly scaled in the current centrifuge test setup.

5.6. Riser inclinations at boundaries

Fig. 14 presents the inclinations at the motion-end and fixed-end. The fixed-end of the riser was slightly affected by the M4 motion as its slope changed from about 1.9° to 2.4°. This change was insignificant and the system performed well.

5.7. Pore pressures

The water level was monitored and maintained using the surface PPTs located at each end of the test box. The riser was fully submerged throughout the test. PPTs 4, 5 and 6 were placed at 28 mm, 42 mm, and 56 mm depth in close proximity to the riser to measure the pore pressure response in the clay during the motions. The motions produced nominal excess pore pressures that dissipated quickly after termination of the motion packets.

5.8. Fatigue stresses

Figs. 15 plots the difference between the maxima and minima (peaks and troughs) in the tension measures at the motion-end by SG1. Despite the increase in overall magnitudes of the tension, the difference between the maximum and minimum values measured remains rather constant during the simple sinusoidal motion of M1. Introduction of a second component to the motion caused some scatter in the difference between maxima and minima as observed during application of M2 with the moving average being the same as that of M1. Interesting to note was the decrease in the magnitude of the difference between maxima and minima tensions during the M3

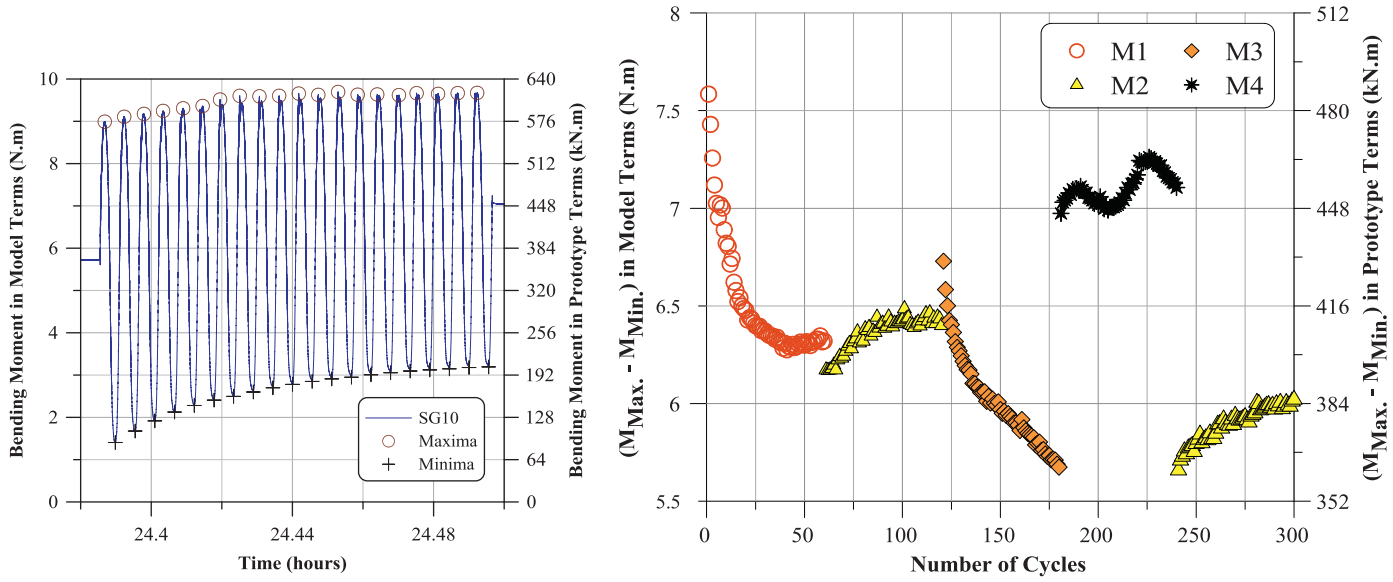

Fig. 9. Bending moments measured by SG10 during M1 motion (left), and SG10 bending moment difference between consecutive maxima and minima versus number of cycles in all motions (right).

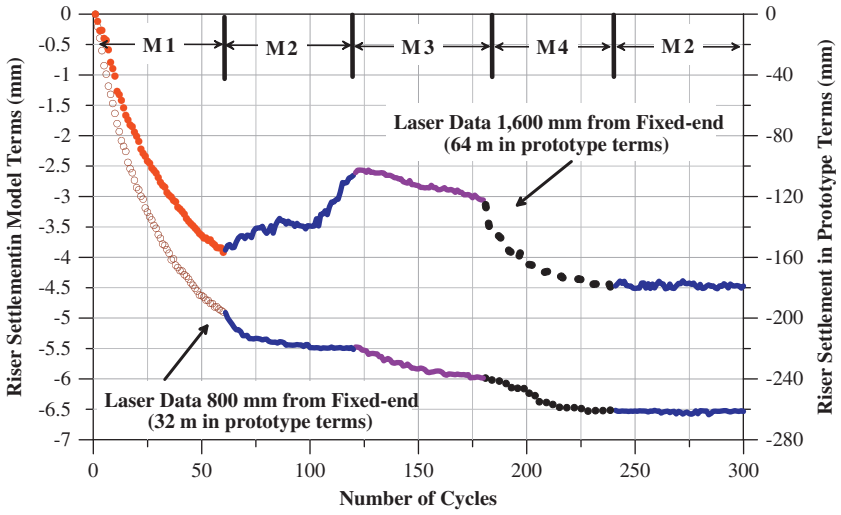

Fig. 10. Laser measurements versus number of applied cycles. These are the deepest measurements in terms of trench depth for each cycle.

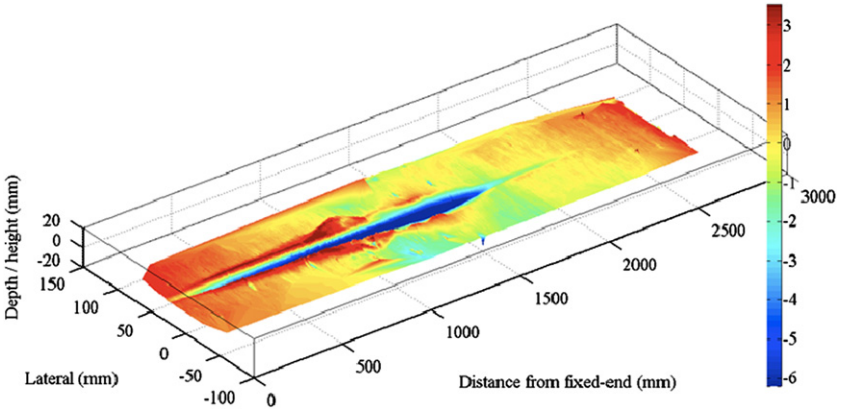

Fig. 11. Three-dimensional view of the final trench geometry. (For interpretation of the references to color in this figure caption, the reader is referred to the web version of this article.)

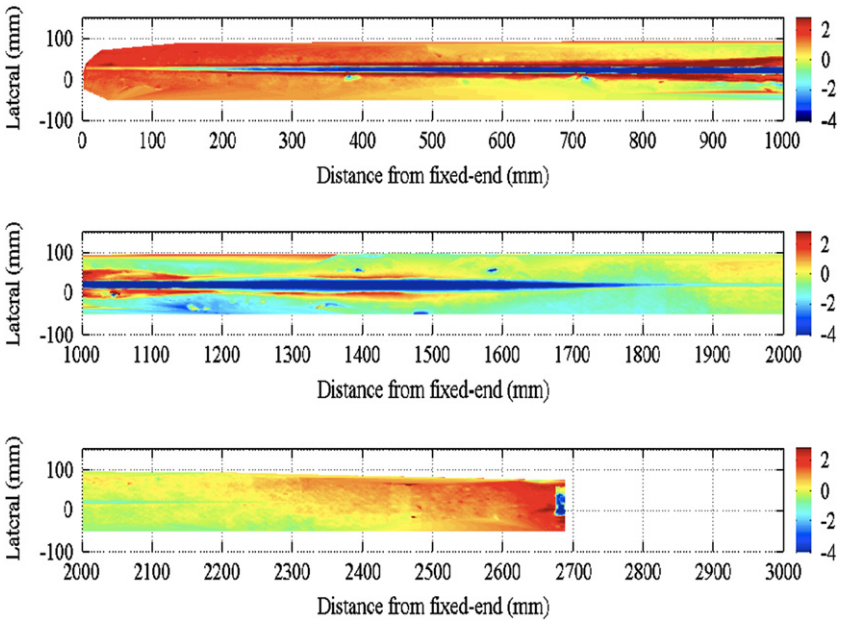

Fig. 12. Plan views of final trench geometry. Zero corresponds to the fixed-end. Lasers were located 800 mm and 1600 mm from the fixed-end. The legend is in model terms. For conversion one needs to multiply by 40. (For interpretation of the references to color in this figure caption, the reader is referred to the web version of this article.)

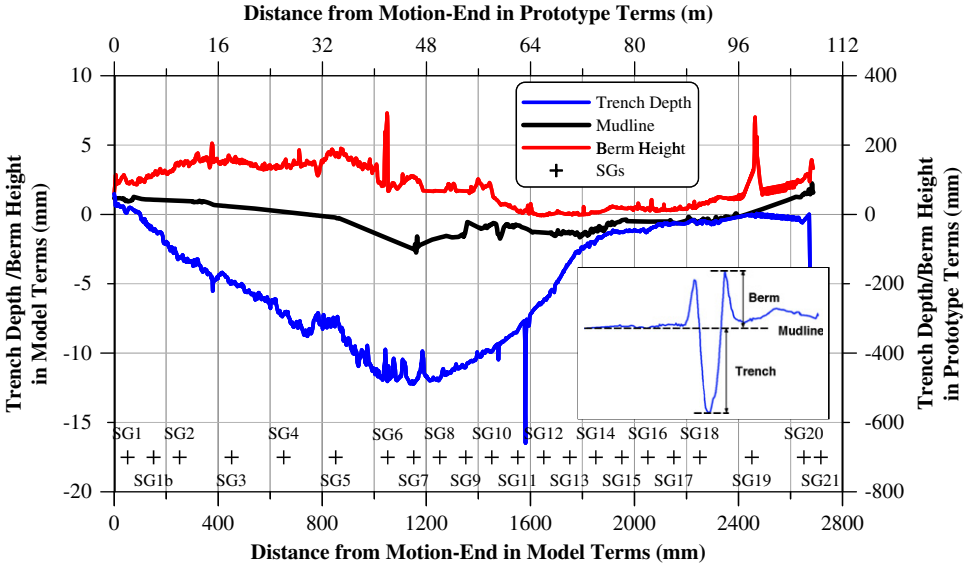

Fig. 13. Final trench base and berm height profiles. The distances are given from the motion-end with the strain gauge locations for the riser resting flat on the model bed.

and M4 motions, which have the RAO characteristics. This decrease was about 7% for the M3 motion and approximately 18% for the M4 motion from commencement. Fatigue from only axial stresses was less of a concern in design of SCRs, however; one needs to consider axial stresses in combination with bending stresses.

Fatigue failure can be regarded as the result of accumulated damage in the material. A simple model of the damage accumulation process is obtained by assuming that each load cycle produces the same amount of damage in the material. This is called the Palmgren–Miner rule of linear cumulative damage. Fatigue life is a non-linear function in conjunction with these stresses. For assessment of high cycle fatigue, fatigue strength is to be calculated based on laboratory tests (S–N curves) or fracture mechanics. It is quite common to use S–N curve for riser applications. The S–N curves to be used for fatigue life calculation may be defined by the following formula:

$$\log N - \log a = m(\log \Delta\sigma)$$

where N is the allowable stress cycle numbers; a and m are parameters defining the curves, which are dependent on the material and structural detail. $\Delta\sigma$ is the stress range including the effect of stress concentration (ABS, 2001). For the tests conducted here, the reduction in the fatigue stress ranges at the critical zone results in a larger number of allowable cycles and therefore, could potentially improve the fatigue life by a considerable amount. It should be noted that a proper fatigue analysis will involve rain-flow counting and consideration of other factor such as material type and appropriate S–N curve and it was not conducted here for the model riser.

Fig. 16 shows the difference between the maxima and minima bending stresses (essentially the fatigue stresses, but these levels require to be factored by power of 3–5 for fatigue life) in SG10 against the numbers of cycles in all motions. Of significant importance was the approximate 20% reduction in the fatigue stresses during the M1 and M3 motions. Both series of M2 motion produced a sparse range of tensions and a slightly increase in the fatigue bending stresses of similar characteristics.

The M4 motion was the largest and therefore, produced the largest fatigue stresses in riser and deepened the trench. Although in terms of the bending stresses it did not show the same trend as the M3, the influence of trench is evident in the tensile stresses. However, the ratio of the stress difference for M4 to stress difference at the end of M3 is less than about 1.25 given that the amplitudes of M4 was 1.5 of those of M3. This also indicates the effect of trench depth in increasing the fatigue life has already taken place. Comparison of the results from the two M2 motions seems to support this argument

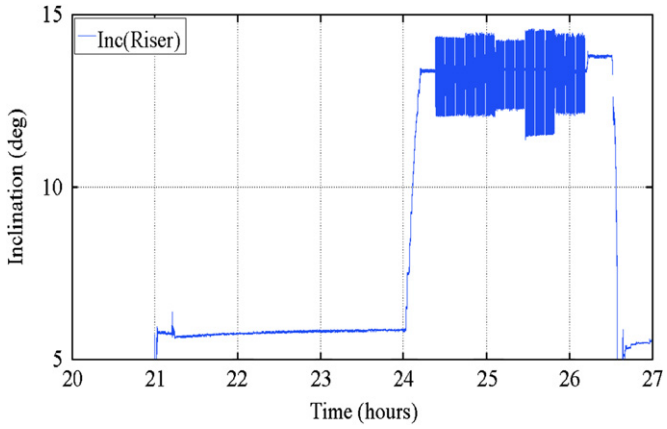

Fig. 14. Riser inclination data at the motion-end with positive showing clockwise rotation.

6. Conclusions

The experimental setup performed very satisfactorily. The test provided valuable insights into various aspects of the fatigue issues related to the SCR's near the touchdown zone. These included trench formation mechanism and its influence on the fatigue life, the fluid–riser–soil interaction mechanism, and pore pressure generated in the vicinity of the riser. The current setup, however, did not fully model the erosive mechanism of the water velocity field on seabed. A number of factors may have contributed to this. For example, the ratio of intact to remolded penetration resistance (which is about two in these tests) is lower than what is typically encountered in the field (3–5 more typical for offshore clays). Another factor is the velocities and frequencies of the motions used, which are about four times slower than those typically encountered in prototype situations. The choice of slower motions was dictated by the equipment capacity. Nonetheless, the topic of erosion scaling in centrifuge is a matter of further investigation.

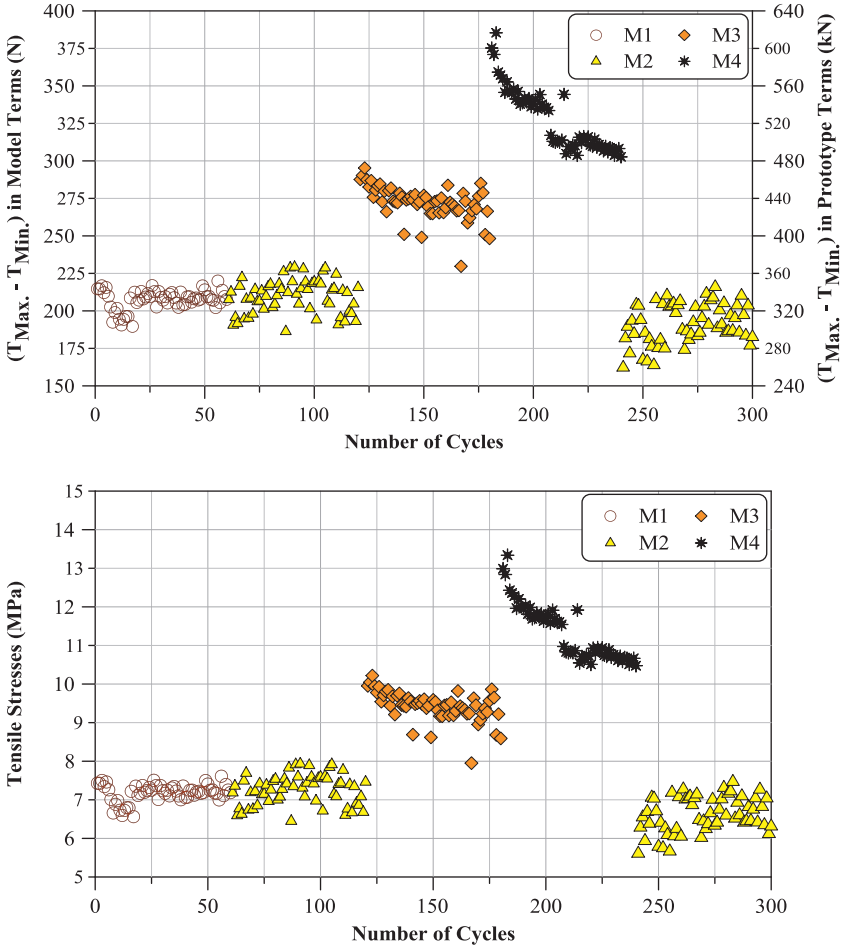

Fig. 15. Difference between maxima and minima tensions in SG1 versus number of cycles (top) and tensile stresses versus number of cycles (bottom).

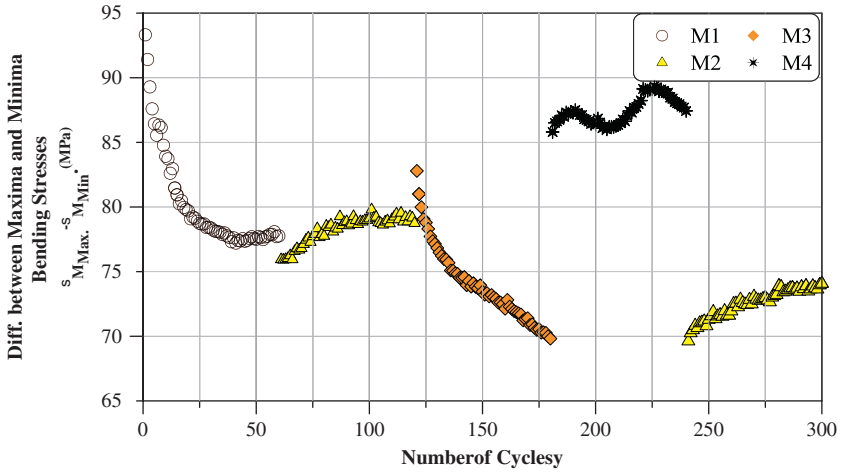

Fig. 16. Difference between consecutive maxima and minima bending stresses in SG10 versus number of applied cycles.

The results demonstrated the trench geometry can have a significant influence on both bending and axial fatigue stresses in a riser. As the trench deepens the fatigue stresses appear to decrease. This decrease in fatigue stresses was about 20% for bending and up to 18% for axial. Base on these results it appears that deepening of the trench can potentially increase the fatigue life of a riser. These observations are in contrast to those reported by others based on tests on a segment of a pipe attempting to simulate riser–soil interaction (Giertsen et al., 2004; Leira et al., 2004) and numerical modeling (Shiri and Randolph, 2010). In addition to deepening of the trench, factors such as softening the trench base and walls could also play a major role. Softening the trench base will reduce the stiffness and increase the damping, which both can affect the fatigue stresses. The trench formation mechanism, geometry and trench base softening and damping, and their effect on the fatigue damages are all subjects of further investigation. The results of this study are encouraging and demonstrated one step forward in the right direction.

Acknowledgments

We are grateful to Don Cameron, Derry Nicholl, and Karl Tuff for their contribution in the development and execution of the centrifuge tests, and to C-CORE for funding the test. We would also like to thank the reviewers for their input to this paper.

References

ABS, 2001. Guide for building and classing subsea pipeline systems and risers. Am. Bur. Shipp., 205.

Aubeny, C.P., Biscontin, G., 2009. Seafloor-riser interaction model. Int. J. Geomech. 9 (3), 133–141.

Elliott, B.J., Zakeri, A., Macneill, A., Phillips, R., Li, G., Clukey, E.C. . Centrifuge modeling of steel catenary risers (SCR's) at Touchdown zone part I: development of novel centrifuge experimental apparatus. Ocean Eng., http://dx.doi.org/10.1016/j.oceaneng.2012.11.012i, this issue.

Finnie, I.M.S., Randolph, M.F., 1994. Punch-through and liquefaction induced failure of shallow foundations on calcareous sediments. In: Proceedings of the International Conference on Behaviour of Offshore Structures, Boston, pp. 217–230.

Giertsen, E., Verley, R., Schroder, K., 2004. Carisima a catenary riser/soil interaction model for global riser analysis. In: International Conference on Offshore Mechanics and Arctic Engineering (OMAE2004), Vancouver, BC, Canada, pp. 633–640.

Lehane, B.M., O'Loughlin, C.D., Gaudin, C., Randolph, M.F., 2009. Rate effects on penetrometer resistance in kaolin. Geotechnique 59 (1), 41–52.

Leira, B.J., Karunakaran, D., Giertsen, E., Passano, E., Farnes, K.-A., 2004. Analysis guidelines and application of a riser–soil interaction model including trench effects. In: International Conference on Offshore Mechanics and Arctic Engineering (OMAE2004), Vancouver, BC, Canada, pp. 955–962.

Shiri, H., Randolph, M.A., 2010. The influence of seabed response on fatigue performance of steel catenary risers in touchdown zone. In: Proceedings of the ASME 2010 29th International Conference on Ocean, Offshore and Arctic Engineering, OMAE2010, Shanghai, China.